JACS
JOURNAL OF THE AMERICAN CHEMICAL SOCIETY

ARTICLE

pubs.acs.org/JACS

Multiple-Filled Skutterudites: High Thermoelectric Figure of Merit through Separately Optimizing Electrical and Thermal Transports

Xun Shi,[†,‡] Jiong Yang,[†] James R. Salvador,[‡] Miaofang Chi,[§] Jung Y. Cho,[‡] Hsin Wang,[§] Shengqiang Bai,[⊥] Jihui Yang,[*,∥] Wenqing Zhang,[*,†] and Lidong Chen[*,⊥]

[†]State Key Laboratory of High Performance Ceramics and Superfine Microstructure, Shanghai Institute of Ceramics, Chinese Academy of Sciences, Shanghai 200050, China

[‡]Chemical Sciences and Materials Systems Lab, General Motors R&D Center, Warren, Michigan 48090, United States

[§]Materials Science and Technology Division, Oak Ridge National Laboratory, Oak Ridge, Tennessee 37831, United States

[⊥]CAS Key Laboratory of Materials for Energy Conversion, Shanghai Institute of Ceramics, Chinese Academy of Sciences, Shanghai 200050, China

[∥]Electrochemical Energy Research Lab, General Motors R&D Center, Warren, Michigan 48090, United States

ABSTRACT: Skutterudites $CoSb_3$ with multiple cofillers Ba, La, and Yb were synthesized and very high thermoelectric figure of merit ZT = 1.7 at 850 K was realized. X-ray diffraction of the densified multiple-filled bulk samples reveals all samples are phase pure. High-resolution scanning transmission electron microscopy (STEM) and energy dispersive X-ray spectroscopy (EDS) analysis confirm that multiple guest fillers occupy the nanoscale-cages in the skutterudites. The fillers are further shown to be uniformly distributed and the Co−Sb skutterudite framework is virtually unperturbed from atomic scale to a few micrometers. Our results firmly show that high power factors can be realized by adjusting the total filling fraction of fillers with different charge states to reach the optimum carrier density, at the same time, lattice thermal conductivity can also be significantly reduced, to values near the glass limit of these materials, through combining filler species of different rattling frequencies to achieve broad-frequency phonon scattering. Therefore, partially filled skutterudites with multiple fillers of different chemical nature render unique structural characteristics for optimizing electrical and thermal transports in a relatively independent way, leading to continually enhanced ZT values from single- to double-, and finally to multiple-filled skutterudites. The idea of combining multiple fillers with different charge states and rattling frequencies for performance optimization is also expected to be valid for other caged TE compounds.

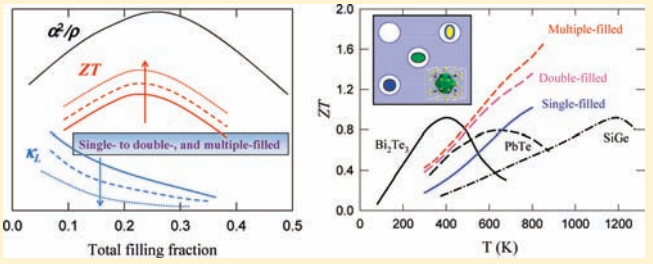

1. INTRODUCTION

Solid-state thermoelectric (TE) technology uses electrons and holes as the working fluid for heat pumping and power generation, and has the virtues of no moving parts and high reliability. Advances in TE materials performance can lead to high thermal-to-electrical energy conversion efficiency and hence significant energy savings by generating electricity from waste heat.[1] The efficiency of TE materials is governed by the dimensionless thermoelectric figure of merit $ZT = \alpha^2 T/\rho\kappa$, where α is the thermopower (Seebeck coefficient), ρ is the electrical resistivity, T is the absolute temperature, and κ is the total thermal conductivity. Though there is no theoretical limit to the value of ZTs, current commercially available materials are still limited to about 1 over their entire operating temperature ranges. To achieve high ZT, one needs to maximize the power factor (PF) α^2/ρ, whereas at the same time minimizing κ. Recent improvements in complex TE materials have led to many advances.[2] Enhanced ZT values have been reported for several classes of materials, including superlattices,[3,4] nanostructured materials,[5,7] and bulk materials.[8−10] However, the transport parameters α, ρ, and κ are usually strongly correlated in materials, which limits the simultaneous optimization of electrical and thermal transports to achieve higher ZTs.

Binary skutterudites, based on the mineral $CoAs_3$ possessing the general formula MX_3 (M = Co, Rh, or Ir; X = P, As, or Sb), have intrinsic nanoscale cages in their crystal structure brought about by corner sharing MX_6 octahedra.[11−13] Among skutterudites, $CoSb_3$ has attracted the greatest interest in waste heat to electricity conversion applications due to its reasonable band gap of ~0.2 eV, high carrier mobility,[13] and the fact that it is composed of inexpensive and environmentally benign constituent elements as compared to other skutterudite materials. The thermal conductivity of the pure binary $CoSb_3$ is, however, too high, which leads to low ZTs and thus poor conversion efficiency for TE applications.[11−13] Filling a large variety of guest atoms,

Received: January 11, 2011
Published: April 27, 2011

such as rare earth,[14−18] alkaline earth,[19−21] alkali metals,[22,23] and other[24−27] ions into the nanocages can form the so-called filled skutterudites. The filling atoms are loosely bound to the Sb host atoms in the intrinsic nanocages, leading to Einstein-like vibrational modes that strongly scatter phonons and significantly reduce the lattice thermal conductivity (κ_L).[28,29] Therefore, the maximum ZTs are significantly improved from 0.5 to 0.8 in doped $CoSb_3$[13] to 1.0−1.1 in single-element-filled skutterudites.[14−23] Recently, the vibrational frequencies of the filler atoms in $CoSb_3$ have been calculated by density functional theory (DFT) and were found to be significantly different for different chemical groups of the periodic table.[30] It was suggested that only the lattice phonons with frequencies near the vibrational frequency of fillers can be strongly scattered via phonon resonant scattering.[9] Therefore, introducing two filler types from different chemical groups into the nanocages of $CoSb_3$ could introduce two distinctive filler vibrational frequencies for a broader range lattice phonon scattering, leading to a further κ_L reduction.[9,30] As a result, the maximum ZTs were improved to 1.3−1.4 in double-element-filled skutterudites.[9,31−34] The maximum ZT in skutterudites is, however, still lower than other state-of-the-art TE materials such as $AgPb_mSbTe_{m+2}$,[7] thus a further optimization to improve ZT in skutterudites is required for real applications.

Here, we present a study on the cofilling of three elements (Ba, La, and Yb) into the nanocages of $CoSb_3$. By carefully selecting the concentration and identity of the filler species, we can introduce scattering centers, which interact with a wider spectrum of phonons, leading to further reduced κ_L. We find that the crystal framework in multiple-filled skutterudites is well-maintained for excellent electrical transport. Therefore, the electrical and thermal transports in multiple-filled skutterudites can be optimized in a relatively independent way, leading to the continually increased ZTs. The maximum ZT in $Ba_uLa_vYb_wCo_4Sb_{12}$ multiple-filled skutterudites reaches 1.7 at 850 K. This is the highest reported value so far for skutterudites and is among the highest for all known bulk TE materials.

2. EXPERIMENTAL SECTION

2.1. Sample Synthesis. Multiple-filled skutterudite samples $Ba_uLa_vYb_wCo_4Sb_{12}$ were synthesized by a combination of induction melting and long-term high-temperature annealing. The high-purity elements Ba (99.99%, piece), La (99.9, rod), Yb (99.9%, piece), Co (99.998%, powder), and Sb (99.9999%, shot) were combined in their stoichiometric ratios and placed in Boron Nitride crucibles, which were then sealed in a fused silica tube, and melted at 1400 °C for 30 s under Ar atmosphere in an induction furnace. The resulting melts were quenched to room temperature, annealed at 750 °C for one week, then ground into fine powders, and cold pressed into pellets followed by annealing at 750 °C for an additional week to ensure homogeneity of all components. The resulting materials were reground into powders and consolidated by Spark Plasma Sintering (SPS) at 650 °C under a pressure of 50 MPa, yielding fully densified bulk samples.

2.2. Structural Characterization. Room temperature powder X-ray diffraction (PXRD) data were collected on a Siemens D5000 diffractometer equipped with Cu Kα radiation (λ = 1.5418 Å) to check the phase purity. Full profile refinements by Rietveld analysis were carried out for two samples using the program *Full-Prof*. The actual compositions were determined by electron probe microanalysis (EPMA) averaged over 12 randomly selected locations via energy dispersive spectrometer (EDS).

2.3. High Angle Annular Dark-Field Scanning Transmission Electron Microscopy (STEM). A Titan 80/300-kV TEM/STEM instrument with a Cs-corrected FEI probe was used to study the microstructure of samples. Bright-field and high-angle annular dark-field (HAADF) STEM images were recorded simultaneously to get full information of the atomic arrangement. TEM specimens were prepared by a traditional method with mechanical polishing followed by low-voltage (1.5 V) ion-milling on a cooling stage. HAADF images were acquired under a 300 kV accelerating voltage and with a convergence angle of 16.8 mrad and a large inner collection angle of 55 mrad. The contrast of the acquired HAADF images thus is Z-sensitive and is used in studying the distribution of filling atoms in this work. Atomic columns are clearly revealed since a beam size of ~0.6 Å was used in this work. The energy dispersive X-ray spectroscopy (EDS) spectra were acquired with the same acquisition time, the same e-beam size of 0.15−0.2 nm and under the same microscope condition.

2.4. Thermoelectric Transport Properties. Hall effect measurements and four-probe resistivity measurements were made in a cryostat with a 5.5 T magnet and a Linear Research ac bridge. Pieces with the dimension of 1 mm × 2 mm × 5.5 mm were cut from the sintered bulk samples for Hall effect and low-temperature resistivity measurements. For a particular magnetic field (B), Hall voltage (ΔV) is calculated by subtracting the voltage at negative field from the value at positive field at a given temperature. By changing the magnetic field, a group of ΔV and B values are obtained. Hall coefficients are then calculated and equal to the slope of the curve ΔV vs B. Electrical resistivity and thermopower from 300 to 850 K were measured using an ULVAC ZEM-3 system. High-temperature thermal conductivity was determined by measuring the thermal diffusivity with an Anter FL5000 laser flash diffusivity instrument. In addition, the specific heat was measured by the ratio method using differential scanning calorimetry performed with a Netzsch DSC 404c with a sapphire reference. The thermal conductivity can then be computed by multiplying specific heat, thermal diffusivity, and density. The high-temperature TE data were checked and remeasured by two established groups (at Oak Ridge National Laboratory and Shanghai Institute of Ceramics) using different instruments. The discrepancies, if any, are less than 3%.

3. RESULTS

3.1. Structural and Compositional Characterizations. PXRD found that all samples were single phase and that each reflection in the powder pattern could be indexed to the cubic $Im\bar{3}$ space group of the parent $CoSb_3$ compound. Rietveld analysis performed on $Ba_{0.09}La_{0.03}Yb_{0.13}Co_4Sb_{12}$ and $Ba_{0.03}La_{0.04}Yb_{0.03}Co_4Sb_{12}$ found that both samples have maintained the body centered space group of the parent. The filler sites (Wyckoff position 2*a*) are populated with Yb atoms and its occupancy was refined followed by its isotropic temperature parameter. For $Ba_{0.09}La_{0.03}Yb_{0.13}Co_4Sb_{12}$ the 2*a* site refined to 20% occupancy (resulting composition $Yb_{0.20}Co_4Sb_{12}$), and $Ba_{0.03}La_{0.04}Yb_{0.03}Co_4Sb_{12}$ refined to approximately 7% occupancy of Yb ($Yb_{0.07}Co_4Sb_{12}$). The isotropic atomic displacement parameters for the filler species were found to be about 1 order of magnitude larger than those of the Co and Sb network atoms, a finding that is consistent with those observed for other partially single-filled skutterudites.[11]

The compositions of the consolidated ingots were determined by EPMA. Table 1 lists the EPMA determined compositions (marked as actual compositions) and room temperature transport properties for all samples investigated.

The grain size distributions were determined to range between a few and 50 μm for all samples as determined by the EPMA backscattered electron (BSE) images. An example BSE image of $Ba_{0.08}La_{0.05}Yb_{0.04}Co_4Sb_{12}$ is shown in Figure 1. The homogeneity of the samples was assessed by averaging the compositions of 12 different grains of each sample (shown in Table 2 for $Ba_{0.08}La_{0.05}Yb_{0.04}Co_4Sb_{12}$) and taking the average. All samples were found to be macroscopically homogeneous.

Table 1. Nominal and Actual Compositions, Density, and Room Temperature Thermal Conductivity, Electrical Resistivity, Thermopower, Electron Carrier Density, and Hall Mobility for $Ba_uLa_vYb_wCo_4Sb_{12}$ Multiple-Filled Skutterudites

nominal composition	actual composition	density [g/cm^3]	κ [W/m·K]	ρ [ohm·m]	α [μV/K]	n [10^{20} cm^{-3}]	μ_H [cm^2/ V·s]
$Ba_{0.06}La_{0.05}Yb_{0.06}Co_4Sb_{12}$	$Ba_{0.06}La_{0.05}Yb_{0.02}Co_4Sb_{12}$	7.38	3.0	5.46×10^{-6}	−138	2.39	48
$Ba_{0.08}La_{0.05}Yb_{0.08}Co_4Sb_{12}$	$Ba_{0.08}La_{0.05}Yb_{0.04}Co_4Sb_{12}$	7.38	2.7	4.17×10^{-6}	−126	3.66	41
$Ba_{0.10}La_{0.05}Yb_{0.10}Co_4Sb_{12}$	$Ba_{0.10}La_{0.05}Yb_{0.07}Co_4Sb_{12}$	7.63	3.1	3.33×10^{-6}	−107	4.95	36
$Ba_{0.10}La_{0.05}Yb_{0.15}Co_4Sb_{12}$	$Ba_{0.09}La_{0.04}Yb_{0.13}Co_4Sb_{12}$	7.67	3.0	3.27×10^{-6}	−104	5.52	41
$Ba_{0.10}La_{0.05}Yb_{0.20}Co_4Sb_{12}$	$Ba_{0.09}La_{0.04}Yb_{0.14}Co_4Sb_{12}$	7.53	3.0	2.97×10^{-6}	−93	7.64	28

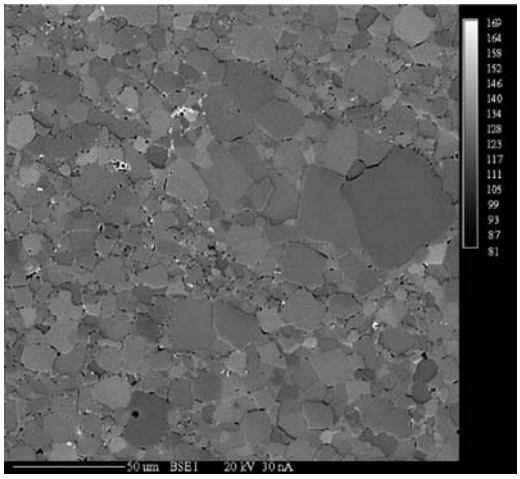

Figure 1. Backscattered electron image of $Ba_{0.08}La_{0.05}Yb_{0.04}Co_4Sb_{12}$. The grains having different shading are attributed to their different crystal orientations. Twelve locations are randomly selected in these skutterudite grains for EPMA analysis. The measured compositions shown in Table 2 demonstrate the skutterudite phase is macroscopically homogeneous.

Lattice parameter as a function of the total filling fraction of the skutterudite phase are plotted in Figure 2, for Ba-filled,[19] Yb-filled,[35] and triple-element-filled skutterudites. The lattice parameter increases with increasing filling fraction for all three series of samples. It is reasonable that data for triple-element filled samples fall in between those of the Ba-filled and the Yb-filled samples since Ba^{2+} has the largest and Yb^{2+} the smallest radius among the three fillers.[36,37]

3.2. Thermoelectric Properties. Density and room temperature thermoelectric properties of multiple-filled skutterudites are shown in Table 1. The relative density for all samples is higher than 96%. It is evident that as the total filling fraction increases, the room temperature resistivity and absolute thermopower decrease. This is an expected result since the fillers donate their valence electrons into the skutterudite framework, leading to *n*-type doping. Hall coefficients for all samples were negative in the temperature range investigated, consistent with the sign of Seebeck coefficient. What is also evident is that as the total filling fraction increases the carrier concentration also increases, confirming that the fillers are effective *n*-type dopants for $CoSb_3$.

Figure 3 shows the room temperature mobility (μ_H) as a function of carrier density (n). Single-, double-, and triple-filled Co_4Sb_{12} possess almost the same μ_H values at a given n. It is around 20 $cm^2V^{-1}s^{-1}$ at an electron concentration of 10^{21} cm^{-3}, 40−50 $cm^2V^{-1}s^{-1}$ at an electron concentration of 5×10^{20} cm^{-3} and 70−80 $cm^2V^{-1}s^{-1}$ at an electron concentration of 10^{20} cm^{-3}. The data for Te and Pd doped $CoSb_3$ are also shown in Figure 3 for comparison. It is clear that the electron mobility of filled $CoSb_3$ is comparable to or slightly higher than unfilled $CoSb_3$ at a given n, indicating that the fillers do not significantly damage the electron transport in skutterudite crystal.

Figure 4 shows the temperature dependence of resistivity, thermopower, and power factor for all samples. The electrical resistivity increases with increasing temperature for all samples, indicating that they are heavily doped semiconductors. All samples have resistivity values less than 1.0×10^{-5} ohm·m at high temperatures and below 6.0×10^{-6} ohm·m at room temperature. The Seebeck coefficients for all samples were negative and increase nearly linearly with increasing temperature up to 850 K, with the exception of $Ba_{0.06}La_{0.05}Yb_{0.02}Co_4Sb_{12}$, reach values of −160 to −190 μV/K at high temperatures. Because of the low total filling fraction of $Ba_{0.06}La_{0.05}Yb_{0.02}Co_4Sb_{12}$ and the resulting low electron carrier density (shown in Table 1), a transition to intrinsic semiconducting transport with both electrons and holes takes place at a temperature around 750 K (shown in Figure 4). Therefore, above this temperature, the absolute value of α decreases, leading to relatively poorer thermoelectric properties due to the mixed electron and hole carrier conduction. The electrical resistivity and thermopower in multiple-filled skutterudites show a trend similar to what was observed in single- and double-filled skutterudites.[9,14−23] It is known that the effective charge state for fillers in $CoSb_3$ is +2 for Ba, and close to +3 for La, +2 for Yb.[39,40] The best performing multiple-filled skutterudites shown in Figure 4 are in the range of the optimum carrier density to achieve high power factors (detail discussion below), which requires 0.4−0.6 electrons per Co_4Sb_{12} unit.[41,42] Most samples show very high power factors >50 $\mu W/cm \cdot K^2$. The maximum power factor for the multiple-filled skutterudites is around 55 $\mu W/cm \cdot K^2$ at 850 K, comparable to the best values in single- and double-filled skutterudites.[9,14−23]

The temperature dependence of specific heat (C_p) is shown in part d of Figure 4. Because of very small composition change in these multiple-filled skutterudites, C_p is very close to each other. It is around 0.21−0.22 $Jg^{-1}K^{-1}$ at 400 K, then slowly increases with increasing temperature, finally reaches 0.22−0.23 $Jg^{-1}K^{-1}$ at high temperatures. We also calculated the specific heat for various single-filled skutterudites using density functional method. The maximum deviation among these single-filled skutterudites is less than 5%. A typical single-filled skutterudite, $Yb_{0.25}Co_4Sb_{12}$, is also shown in part d of Figure 4. At high temperatures, C_p of $Yb_{0.25}Co_4Sb_{12}$ single-filled skutterudites is very close to those of the multiple-filled skutterudites. The maximum discrepancy in the whole temperature is around 5%, demonstrating these partially filled skutterudites possess similar specific heat values at high temperatures. The total thermal conductivities in the range of 300 to 850 K for multiple-filled skutterudites are shown in Figure 5 and the room temperature values are listed in Table 1. All samples have very similar values at room temperature (around 3 W/m·K). At higher temperatures, the thermal conductivity values are almost constant or

dx.doi.org/10.1021/ja111199y |*J. Am. Chem. Soc.* 2011, 133, 7837–7846

Table 2. Percent Atomic Composition of $Ba_{0.08}La_{0.05}Yb_{0.04}Co_4Sb_{12}$ at 12 Randomly Selected Locations[a]

elements	atomic percent concentration (normalized to 100%)											
Ba	0.49	0.49	0.48	0.54	0.43	0.56	0.52	0.50	0.54	0.51	0.54	0.48
La	0.30	0.31	0.27	0.27	0.33	0.34	0.31	0.28	0.24	0.34	0.32	0.29
Yb	0.19	0.19	0.23	0.23	0.22	0.23	0.23	0.19	0.20	0.23	0.24	0.23
Co	24.76	24.58	24.72	24.67	24.74	24.64	24.67	24.56	24.69	24.95	24.54	24.66
Sb	74.26	74.43	74.30	74.35	74.32	74.25	74.32	74.47	74.33	74.00	74.39	74.35

[a] All the numbers are normalized to 100%.

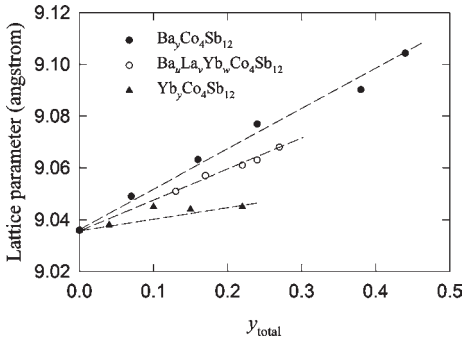

Figure 2. Lattice parameter as a function of the total filling fraction for Ba-filled, Yb-filled, and triple-element-filled skutterudites.

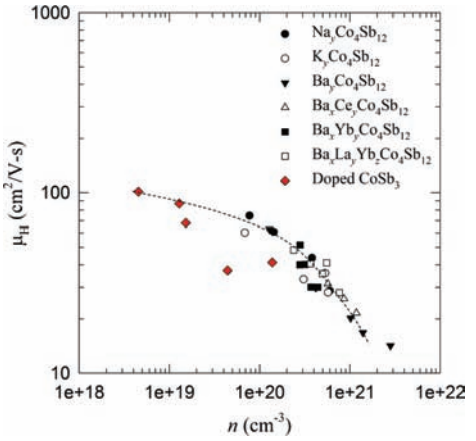

Figure 3. Carrier density dependence of electron mobility in partially filled skutterudites. The dashed line is a guide to the eye. Data for single- and double- filled skutterudites are taken from refs 7−14. Data for doped $CoSb_3$ are taken from ref 38.

slowly increase with increasing temperature. No clear filling fraction dependence is observed. This is because the electronic contribution is a significant portion of the total thermal conductivity in the multiple-filled skutterudites studied here. The lattice thermal conductivity is calculated by subtracting the electronic part from the total thermal conductivity (shown below) and is shown to decrease when increasing total filling fraction.

The temperature dependence of ZT is shown in part b of Figure 5. The ZTs for all samples increase with increasing temperature, range from 0.29 to 0.43 at room temperature, and reach 1.3 to 1.7 at 850 K. The maximum ZT reaches 1.7 in triple-filled skutterudites. Considering that fact that maximum ZT was improved from 0.5 in unfilled Co_4Sb_{12}[13] to 1.1 in single-filled,[16,19] and to 1.3−1.4 in double-filled systems,[9,31−34] we have firmly demonstrated that filling, especially the multiple element filling, is an effective method to enhance the thermoelectric figure of merit. The ZT of 1.7 is the highest reported value so far in skutterudites and is one of the highest values reported for bulk TE materials, suggesting that multifilled skutterudites have great potential for industrial applications.

4. DISCUSSIONS

4.1. Optimization of Electrical Transports: Optimum Electron Density and Maximum Power Factors in Partially Filled $CoSb_3$. It is believed that the electrical transport in partially filled $CoSb_3$ is mainly confined to the Co−Sb framework and the filler atoms only slightly change the conduction band edge.[40,41] The (unperturbed) skutterudite framework and uniform component distribution on the micrometer scale have been shown in Figure 1. The atomistic level structural features were experimentally verified in the multiple-filled skutterudites by high-resolution STEM measurements (Figure 6). We chose images along the [111] orientation for easier visualization, since the atomic columns containing filler atoms are better isolated from their neighboring columns in this projection. Figure 6 shows a HAADF STEM image of $Ba_{0.08}La_{0.05}Yb_{0.04}Co_4Sb_{12}$ multiple-filled skutterudite in the [111] direction. A uniform and highly crystalline skutterudite framework is clearly shown. Combined with Figure 1, it is clear that the skutterudite phase is very uniform and that the Co−Sb framework is well maintained in the multiple-filled skutterudites from the atomic level to micrometer length scale.

A defect-free $CoSb_3$ is a very good intrinsic semiconductor with low carrier density on the order of 10^{16}−10^{17} cm^{-3}.[43] The filler atoms inside the voids of $CoSb_3$ donate their valence electrons into the $CoSb_3$ framework to make the system a heavily doped semiconductor with high carrier density on the order of 10^{20} cm^{-3}.[40] In partially filled $CoSb_3$, the electron density could be easily adjusted by changing the filling fraction of the guest atoms. Notice that each type of filler atom has different charge state and usually the valence electrons are not completely transferred due to the mixed ionic and covalent bond character between the fillers and the surrounding Sb atoms of the first coordination sphere although the chemical bond is mainly ionic.[39,40] Also, because the band structure around the Fermi level in $CoSb_3$ is almost unchanged by the extra filler atoms,[39−41] the effect of fillers on electrical transport properties is only to increase the electron concentration, which is predominantly determined by the filling fraction and ionic charge state of the fillers in $CoSb_3$. In general, a multiple-filled skutterudite could be written as $(G_1)_{y_1}(G_2)_{y_2}...(G_n)_{y_n}Co_4Sb_{12}$, where y_n is the filling fraction of the n^{th} guest atom (G_n) with the effective charge state q_n. Using the estimated charge state q_n[40] of the fillers in $CoSb_3$, electron density as a function of $(\Sigma_{i=1}^{n}(q_i \times y_i))$ is shown in Figure 7. The electron density increases with increasing total filling fraction. Furthermore, single-, double-, and multiple-filled skutterudites show a similar trend, consistent with the picture that the filler atoms only slightly change the conduction band edge of $CoSb_3$.[40,41] This figure clearly demonstrates that the carrier density in partially double- and

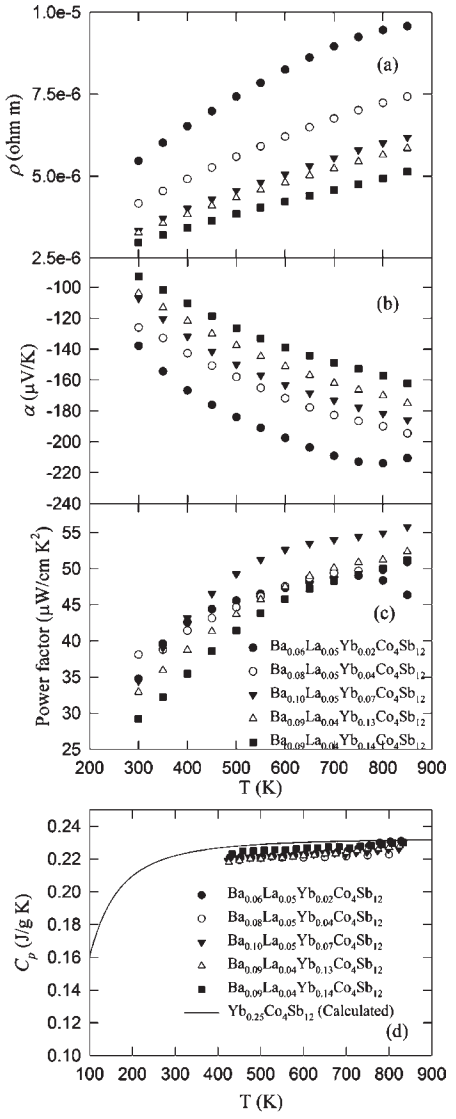

Figure 4. Temperature dependence of (a) electrical resistivity, (b) thermopower, (c) power factors, (d) specific heat for $Ba_uLa_vYb_wCo_4Sb_{12}$ multiple-filled skutterudites. The calculated specific heat for $Yb_{0.25}Co_4Sb_{12}$ single-filled skutterudite is also shown in (d) for comparison.

multiple-filled $CoSb_3$ could be well controlled by adjusting the filling fractions of different type of fillers with different effective charge states. The knowledge of the effective charge states of those fillers in $CoSb_3$ from our earlier work[39,40] is helpful in search for systems with optimal carrier density. The high power factor region (see details below) is also shown in Figure 7, where $(\Sigma_{i=1}^{n}(q_i \times y_i))$ corresponds to the donated electrons by the fillers per Co_4Sb_{12}. It is very clear that in order to obtain high power factors in partially filled $CoSb_3$, the optimum number of electrons in a Co_4Sb_{12} unit should range from 0.33 to 0.7, consistent with theoretical calculations.[41] Therefore, if the average effective charge state (q_v) of the fillers from different chemical groups in multiple-filled skutterudites is +1, the optimum total filling fraction (y_{total}) should be between 0.33 and 0.7; If q_v is +2, the optimum y_{total} is from 0.18 to 0.35; and if q_v is +3, the optimum y_{total} is from 0.11 to 0.23.

Generally, when increasing carrier density in a material, thermopower decreases and electrical resistivity degreases, leading to an optimized carrier density corresponding to the highest power factor for a given bulk semiconductor. We have shown that the optimum carrier density at room temperature should be around 6×10^{20} cm^{-3} in single- and double-filled skutterudites.[42] Our Ba−La−Yb multiple-filled skutterudites also agree with this being the optimum electron density value. Figure 8 shows the power factors at 850 K as a function of electron density (room temperature value) for single-, double-, and multiple-filled skutterudites. We found that the highest PF is around 55 μW/cm-K^2, corresponding to a room temperature electron concentration (n) value of around 10×10^{20} cm^{-3}. It should be noted that the high PFs above 50 μW/cm-K^2 are distributed in a broad range of n ranging from 6×10^{20} cm^{-3} to 12×10^{20} cm^{-3} at 850 K, indicating a wide space for electrical transport optimization. The optimum theoretical electron density was calculated by DFT and was found to be between 0.4 and 0.6 electrons per Co_4Sb_{12} at 850 K.[41] If we assume that the pure defect-free $CoSb_3$ is an intrinsic semiconductor, the electron density in partially filled-skutterudites is mainly from electrons donated from the filler atom. Therefore, 0.4−0.6 electrons per Co_4Sb_{12} correspond to an electron density of $10-16 \times 10^{20}$ cm^{-3}. The calculated PFs for single Ba- and Yb-filled skutterudites are also plotted in Figure 8. The effective charge states reported in ref 40 are used for electron density calculations. An electron relaxation time (τ) of 1.5×10^{-14} s is utilized to estimate power factors based on the calculated $\alpha^2/\rho\tau$ shown in ref 41 for comparison of theory with experiment. Notice that the range of optimum carrier density for maximum power factors based on calculations coincide with experimental data, which is actually independent of the relaxation time used. Taking into account the measurement errors, the calculated values agree well with the experimental observations, confirming our reported optimum electron density in partially filled skutterudites. In addition, consistent with the room temperature trends shown in ref 42, single-, double-, and multiple-filled skutterudites all follow in similar fashion at 850 K, further corroborating that the use of various fillers only weakly affect the electrical transports. On the basis of these results and analysis, once one knows the filler atom type and effective charge state, it is very easy to obtain high PFs in partially filled skutterudites through accurately tailoring the filling fractions.

4.2. Optimization of Thermal Transports: Reduced Lattice Thermal Conductivity via Multiple Fillers with Nonoverlapping Vibrations in the Intrinsic Nano Cages. High-resolution STEM images of $Ba_{0.08}La_{0.05}Yb_{0.04}Co_4Sb_{12}$ are shown in Figure 9 to clearly illustrate the distribution of fillers. To isolate the filler intensity in a STEM image and simplify interpretation, the images along the [001] direction are shown for multiple-filled skutterudites (Figure 9), where the filler-only atomic columns are clearly revealed. The distribution of guest fillers can be probed along the [001] direction where filler-only atomic columns can be identified. The large intensity fluctuation among these atomic columns indicates the random distribution of the fillers in the voids. Compared to the homogeneous intensity of Sb or Co atomic columns, the significant intensity fluctuation among the columns of atomic fillers indicates a random distribution of the fillers in the voids of the skutterudite (part c of Figure 9).

Three energy dispersive X-ray spectroscopy (EDS) spectra randomly acquired from more than 20 positions were compared. These spectra were acquired with the same acquisition time, the same e-beam size of 0.15−0.2 nm, and under the same microscope condition. The intensities of Sb and Co peaks are the same in all locations. The variation of the peak intensities of filling elements (for example Yb) in different spectra indicates a random distribution of

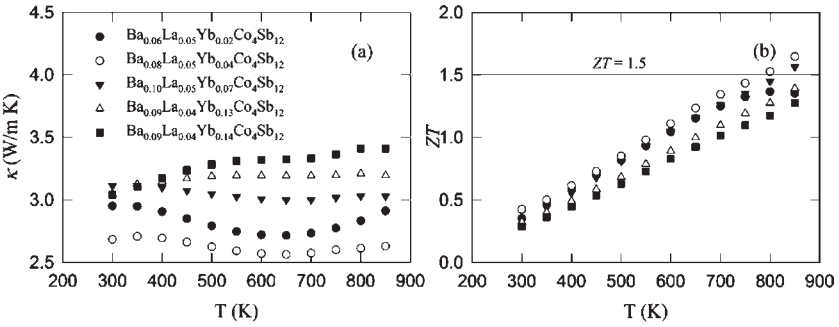

Figure 5. (a) Temperature dependence of total thermal conductivity, and (b) temperature dependence of ZT for $Ba_uLa_vYb_wCo_4Sb_{12}$ multiple-filled skutterudites.

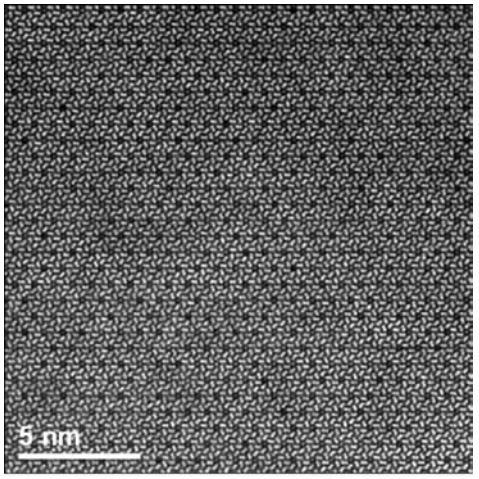

(a)

Figure 6. Typical high-angle annular dark-field STEM (HAADF-STEM) image of $Ba_uLa_vYb_wCo_4Sb_{12}$ multiple-filled skutterudites along the [111] orientation.

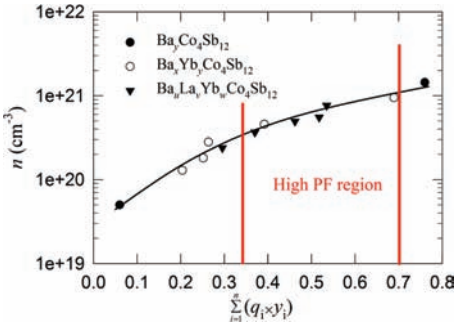

Figure 7. Carrier density as a function of $(\Sigma_{i=1}^{n}(q_i \times y_i))$ for partially filled $CoSb_3$, where q_i is the effective charge state and y_i is the filling fraction of the i^{th} filler in multiple-filled skutterudites. The solid black line is a guide to the eye. The red lines enclose the estimated high power factor region (details below).

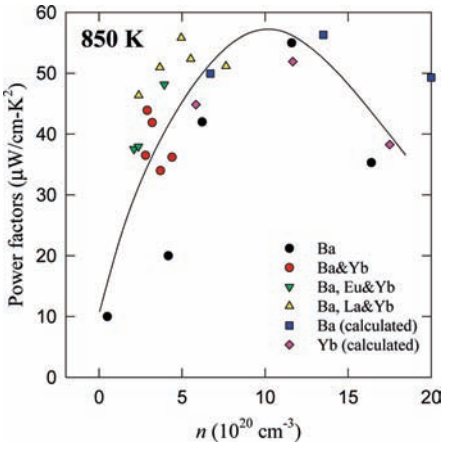

Figure 8. Power factors at 850 K as a function of room temperature carrier density for single-, double-, and multiple-filled skutterudites. The solid line shows a trend for both the calculated and measured data.

the fillers within the narrowly defined region. The low intensity of La and Ba is mainly because of the small beam size used for our EDS acquisition. Such a small beam is used for a highly localized EDS analysis to reveal the uneven distribution of fillers within the grain. However, the peaks of La and Ba are well separated from the signal of Sb, and the spectrum shows the existence of both La and Ba although the signal-to-noise is weak (Figure 10).

STEM and EDS results indicate that filler atoms are filled randomly into the crystallographic voids of the skutterudite without significant perturbation of the Co−Sb network. This is an important result as it shows that the electrical transport is not deteriorated by the introduction of filler atoms. This argument is further confirmed by our electron mobility data shown in Figure 3, where the values in the filled $CoSb_3$ are comparable to or slightly higher than those of unfilled $CoSb_3$ at a similar electron concentration. In most other material systems it is often the case that the addition of impurities to alter the carrier concentration, generally also leads to carrier mobility reduction by alloy and strain field scattering. Skutterudites are therefore unique such that κ_L can be reduced by the introduction of multiple guest atoms without deteriorating the power factor. Our strategy is to optimize the filling fractions with various charge states to obtain the optimum carrier concentration range for high PFs, while at the same time combine multiple fillers of different rattling frequencies to achieve broad-spectrum phonon scattering for low thermal conductivity. Compared with point defect scattering, filler-induced phonon resonant scattering is the dominant phonon scattering mechanism in filled-skutterudites.[44] It was suggested that only lattice phonons with frequencies similar to those of the vibrational modes of the filler atoms in the cages could be strongly scattered by phonon resonant

dx.doi.org/10.1021/ja111199y |J. Am. Chem. Soc. 2011, 133, 7837–7846

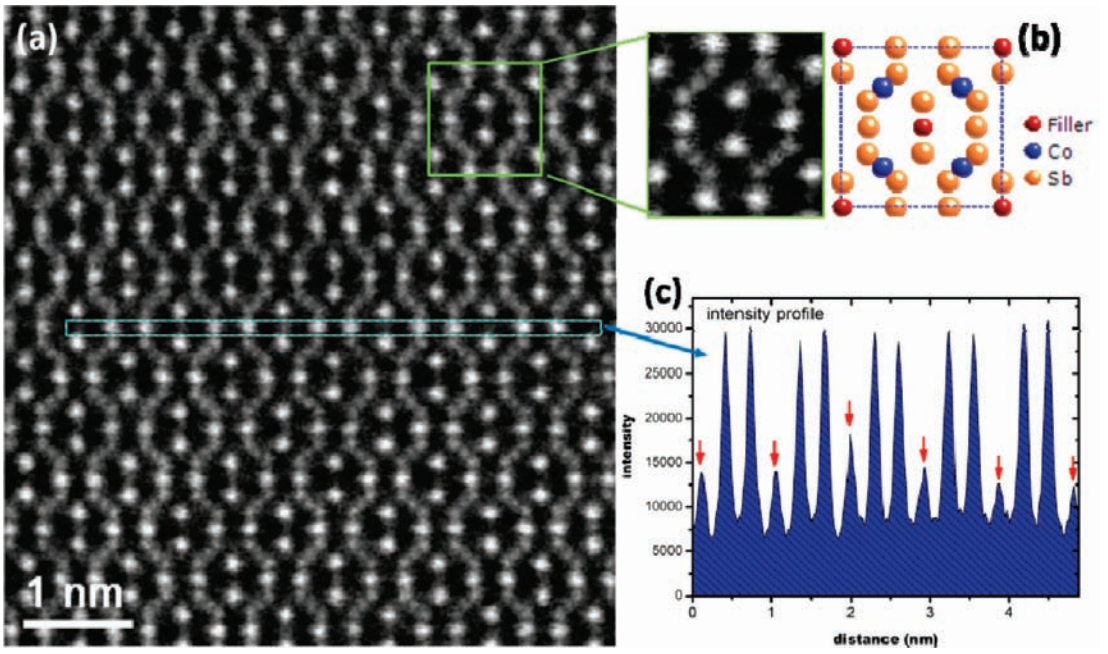

Figure 9. A typical HAADF-STEM image of $Ba_{0.08}La_{0.05}Yb_{0.04}Co_4Sb_{12}$ multiple-filled skutterudite along [001] orientation (a), its detailed atomic arrangement is illustrated in (b), an intensity profile along the box marked in (a) is shown as an example displaying the intensity variation among the filler-only atomic columns compared to the homogeneous intensity profile of the neighbor Sb atomic columns.

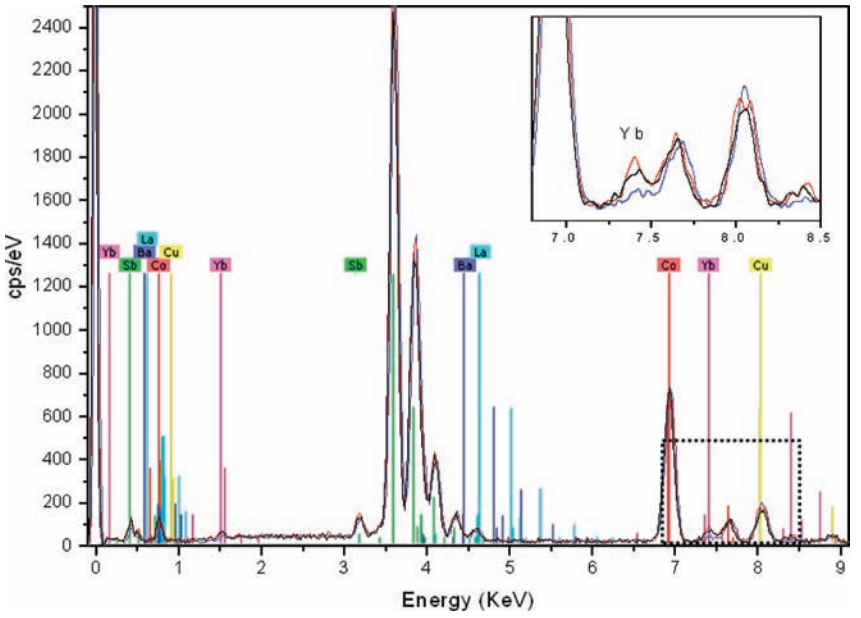

Figure 10. Three EDS spectra for $Ba_{0.08}La_{0.05}Yb_{0.04}Co_4Sb_{12}$. The insert shows the peaks of Yb fillers. The variation of the peak intensities in different spectra indicates random distribution of the fillers. (Cu signal is from the TEM Cu supporting grid).

scattering.[9] Therefore, in order to maximize the phonon resonant scattering in double- and multiple-filled skutterudites, filler elements with large contrasts in their vibrational frequencies from different chemical groups are recommended (shown in Figure 11). The calculated vibrational frequencies of the fillers in $CoSb_3$ using DFT were reported in ref 30. The experimental values, measured by inelastic neutron scattering,[45] agree well with those calculated, as shown in Figure 11.[45] The sharp increase in scattering intensity above 10 meV is attributed to Sb vibrations in the skutterudite framework. Furthermore, when the total filling fraction is less than 0.29, the fillers are believed to behave as phase-incoherent Einstein oscillators and the localized vibrational frequencies induced by the fillers remain unchanged in multiple-filled skutterudites.[45] Therefore, on the basis of the calculations, to maximize the resonance scattering of lattice phonons as much as possible, Ba—Yb were initially selected for making double-filled skutterudites[9] because they have the largest contrast in vibrational frequencies, with the exception of alkali

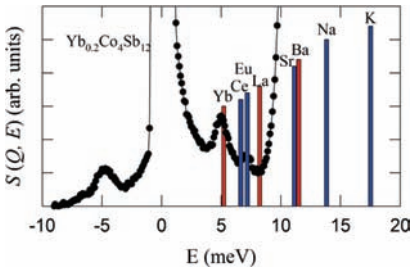

Figure 11. Dynamic scattering function $S(Q, E)$ as a function of energy for $Yb_{0.2}Co_4Sb_{12}$. The solid columns represent the calculated values for fillers in $CoSb_3$ taken from ref 30.

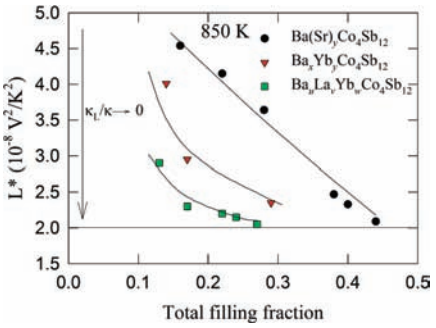

Figure 12. Effective Lorentz number L^* as a function of total filling fraction at 850 K in partial filled skutterudites. The black solid lines are guides to the eye.

metals, and Ba−La−Yb combinations were selected to form multiple-filled skutterudites because the vibrational frequency of La is in between those of Ba and Yb. All calculated values of other fillers are also shown in Figure 11. This demonstrates that a wide range of lattice phonons can be resonantly scattered by appropriately selected double and multiple fillers. Note that the measured vibrational frequencies of the filler atoms are distributed in a narrow energy region as a localized peak. If multiple elements with similar vibrational frequencies are selected as guest atoms the reduction in thermal conductivity will not be as great due to the spectral overlap and therefore a narrower range of phonons being scattered, than would be possible if a more appropriate combination was chosen.

Lattice thermal conductivity κ_L is calculated by $\kappa_L = \kappa - \kappa_e$, where κ_e is the electronic thermal conductivity. κ_e is calculated by $\kappa_e = L_0T/\rho$, where L_0 is the Lorentz number. Typically Lorentz numbers equal to 2.45×10^{-8} and 1.49×10^{-8} V^2/K^2 are used for metals and intrinsic semiconductors, respectively. The Lorentz number for skutterudites (heavily doped semiconductors) should fall in between these two limits. The Lorentz number can be calculated using *ab initio* method, together with the Boltzmann transport theory. Readers can refer to refs 46−48 for detailed methodology. Our calculations show that the Lorentz number for *n*-type skutterudites is approximately 2.0×10^{-8} V^2/K^2. This is the value we used to calculate the electronic contribution to thermal conduction in the article. This value is also supported by our experimental data. For example if we assume that the heat conduction in filled skutterudites at high temperatures is strictly from the electrons, the effective Lorentz number (L^*) can be obtained by $L^* = \kappa\rho/T$. When κ_L is close to zero, L^* is close to the actual Lorentz number (L_0). The calculated L^* in partial filled Co_4Sb_{12} is shown in Figure 12 and we find that L^* approaches 2.0×10^{-8} V^2/K^2 when κ_L approaches zero, particularly for double- and multiple-filled skutterudites. The calculated L_0 value is also consistent with ref 48 and Dyck's calculations for Ba partially filled Co_4Sb_{12} using a mixed carrier scattering model.[49]

Parts a and b of Figure 13 show the room temperature and the high-temperature thermal conductivity respectively versus the total filling fraction for single-,[17,19] double-,[9,31] and triple-filled skutterudites. The value of κ_L in multiple-filled skutterudites is between 1 and 2 (W/m-K) at room temperature. Above 850 K, κ_L is reduced to around 0.20 (W/m-K) when the total filling fraction is >20% as shown in part b of Figure 13. The κ_L is therefore less than 10% of the total thermal conductivity. Using the method reported by Cahill,[50] the calculated minimum thermal conductivity (κ_{min}) is around 0.52−0.54 W/m-K from room temperature to 850 K, comparable to the value (about 0.45 W/m-K) using equation $\kappa_{min} = 1/3C_v\nu l_{min}$, where C_v is the specific heat per volume, ν is the sound velocity, and l_{min} is the minimum phonon mean free path, equal to the nearest interatomic distance. This method is based on a random walk between Einstein oscillators, of varying sizes through subdividing the sample volume into subgroups of atoms. If we use Einstein's original concept,[51] the oscillators are considered to be solely individual. In this case, the calculated thermal conductivity (κ_{Eins}) is about 0.2W/m-K above room temperature with an Einstein temperature of 150 K[52] in partially filled skutterudites. This value is very close to the lattice thermal conductivity in our multiple filled skutterudites (part b of Figure 13), and also consistent with the value (about 0.23 W/m-K) using equation $\kappa_{min} = 1/3C_v\nu l_{min}$, where l_{min} is half of the nearest interatomic distance (1.26 Å). This means that the phonon mean free path in our multiple-filled skutterudites approaches the order of half of the nearest neighbor interatomic distance. Furthermore, a significant κ_L reduction is observed for skutterudites when progressing from single-filled to double- and finally to multiple-filled materials. As the number of filler types increases, κ_L decreases for any given total filling fraction. This is consistent with our understanding that the fillers in double- and multiple-filled skutterudites are selected to have nonoverlapping phonon densities of states peaks in order to ensure a broader range of phonon scattering as the number of filler types is increased. Also note that κ_L in Ba−Yb double-filled skutterudites is lower than that in Ba−Ce double-filled skutterudites at both room and high temperatures at any given total filling fraction because of the small frequency contrast in Ba−Ce double-filled skutterudites. Because of the similar filler resonant frequencies of Sr and Ba,[30] the ZT values in Sr−Ba−Yb filled skutterudites in ref 53 is comparable to double-filled skutterudites and lower than our multiple-filled skutterudites, which further confirms our aforementioned arguments and conclusions. Besides phonon resonant scattering, point defect scattering by the fillers also plays an important role in the reduction of κ_L.[44] In pure $CoSb_3$, the mass contrast between the fillers and the voids is very large. A recent study showed that a stronger point defect scattering by the fillers is observed in double-filled skutterudites as compared with single-filled due to the extra mass fluctuation at the void sites.[54] However, the extra point defect scattering by two types of fillers may not be as strong as that shown in ref 54 because of the small mass fluctuation between the fillers used in our studies. This effect might be further weakened in multiple-filled skutterudites for the same reason. Therefore, the κ_L reduction in multiple-filled

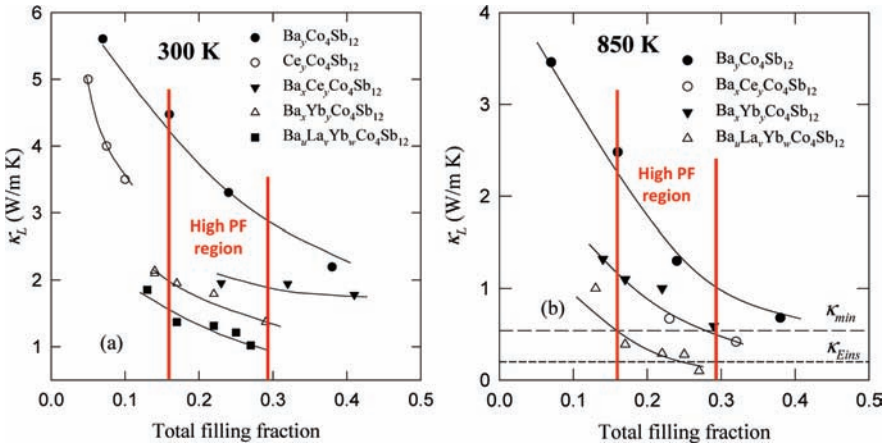

Figure 13. (a) Room temperature and (b) high-temperature (850 K) lattice thermal conductivity as a function of total filling fraction. The solid lines are guides to the eye. Estimated high power factor region (between the red lines) are also shown to demonstrate how to simultaneously maximize power factors and minimize lattice thermal conductivity.

skutterudites is mainly attributed to extra phonon resonant scattering by the fillers with nonoverlapping frequencies, which is also consistent with or confirmed by our experimental data. The optimum electron density in partially filled skutterudites for high PFs has been demonstrated above. The corresponding total filling fraction is also shown in Figure 13 based on simple electron-counting using the effective charge states of the fillers. It is clear that we can simultaneously adjust the total filling faction to be in the high PF region and fill multiple rattlers to get steadily lower lattice thermal conductivity.

4.3. Design for High ZTs: Continually Enhanced Performance from Single- to Double-, and Finally Multiple-Filled $CoSb_3$. As we demonstrated above, in partially filled $CoSb_3$, high PFs could be achieved by adjusting the total filling faction for optimizing carrier density, and κ_L could be continually decreased through the filling of carefully selected guest atoms with nonoverlapping localized vibrational modes. The random filler atom distribution and the unperturbed skutterudite framework are evident from the atomic scale to a few micrometers. Introducing double- and multiple-fillers into the skutterudite only affects the intrinsic cages without any perturbation to the framework atoms. Therefore, double- and multiple-filled skutterudites show a unique possibility to separately optimize electrical and thermal transport properties for high ZTs. One can start by designing a composition with proper total filling fraction close to the optimum carrier density for high PFs, then select two or more types of fillers to be filled into the intrinsic nanocages to decrease κ_L while maintaining the appropriate carrier density value. As a result, the ZTs would be continually increased from single- to double-, and finally multiple-filled skutterudites, which is demonstrated by our experimental data shown above.

5. CONCLUSIONS

Bulk $Ba_uLa_vYb_wCo_4Sb_{12}$ multiple-filled skutterudites have been synthesized by combing induction melting, high-temperature annealing, and spark plasma sintering. Their thermoelectric properties are studied from room temperature to 850 K. Backscattered electron and STEM images clearly show the unperturbed skutterudite Co−Sb framework atoms from the atomic level to a few micrometers. High-resolution STEM, and EDS analysis reveal that the multiple guest atoms randomly occupy the nanocages in the skutterudite structure. Therefore, the unique crystal structure of the skutterudite allows the independent optimization of the electrical and thermal transport properties when the voids are partially filled. Electron concentration in partially filled $CoSb_3$ could be easily controlled via adjusting total filling fraction to reach the optimum value for high power factors. The lattice thermal conductivity in partially filled $CoSb_3$ could be continually reduced via multiple fillers with nonoverlapping vibrational frequencies. As a result, the ZTs are continually increased in double- and multiple-filled skutterudites. The maximum ZT is improved to 1.7 at 850 K for $Ba_{0.08}La_{0.05}Yb_{0.04}Co_4Sb_{12}$, which is the highest value reported in skutterudites. Filled skutterudites possess many advantageous attributes for TE applications, including good mechanical properties and thermal stability,[56,56] are composed of readily available elements, and can be doped such that of both *n*- and *p*-type material can be made, which is optimal for module construction. The ZT improvements we demonstrate make these materials very attractive for power generation applications. Some of the ZT improvement methods we used may be specific to the skutterudite compounds, we expect, nevertheless, the general methodology developed in this study should be applicable to other thermoelectric materials with cage structures.

AUTHOR INFORMATION

Corresponding Author

jihui.yang@gm.com; wqzhang@mail.sic.ac.cn; cld@mail.sic.ac.cn

ACKNOWLEDGMENT

This work is supported by GM and by DOE under corporate agreement DE-FC26-04NT42278, by the Assistant Secretary for Energy Efficiency and Renewable Energy, Office of Transportation Technologies as part of the High Temperature Materials Laboratory User Program at Oak Ridge National Laboratory managed by the UT-Battelle LLC, for the Department of Energy under contract DEAC05000OR22725, and by National Basic Research Program of China (973-program) under Project No. 2007CB607503 and NSFC projects (50825205, 50672118, 50821004, 50820145203, and 10634070). Microscopy research

is supported by ORNL's Shared Research Equipment (SHaRE) User Facility, which is sponsored by the Office of BES, U.S. DOE.

REFERENCES

(1) Yang, J.; Caillat, T. *MRS Bull.* **2006**, *31*, 224.
(2) Snyder, G. J.; Toberer, E. S. *Nat. Mater.* **2008**, *7*, 105.
(3) Venkatasubramanian, R.; Siivola, E.; Colpitts, T.; O'Quinn, B. *Nature* **2001**, *413*, 597.
(4) Harman, T. C.; Taylor, P. J.; Walsh, M. P.; LaForge, B. E. *Science* **2002**, *297*, 2229.
(5) Poudel, B.; Hao, Q.; Ma, Y.; Lan, Y. C.; Minnich, A.; Yu, B.; Yan, X.; Wang, D. Z.; Muto, A.; Vashaee, D.; Chen, X. Y.; Liu, J. M.; Dresselhaus, M. S.; Chen, G.; Ren, Z. *Science* **2008**, *320*, 634.
(6) Zhou, M.; Li, J. F.; Kita, T. *J. Am. Chem. Soc.* **2008**, *130*, 4527.
(7) Hsu, K. F.; Loo, S.; Guo, F.; Chen, W.; Dyck, J. S.; Uher, C.; Hogan, T.; Polychroniadis, E. K.; Kanatzidis, M. G. *Science* **2004**, *303*, 818.
(8) Sales, B. C.; Mandrus, D.; Williams, R. K. *Science* **1996**, *272*, 1325.
(9) Shi, X.; Kong, H.; Li, C. P.; Uher, C.; Yang, J.; Salvador, J. R.; Wang, H.; Chen, L.; Zhang, W. *Appl. Phys. Lett.* **2008**, *92*, 182101.
(10) Heremans, J. P.; Jovovic, V.; Toberer, E. S.; Saramat, A.; Kurosaki, K.; Charoenphakdee, A.; Yamanaka, S.; Snyder, G. J. *Science* **2008**, *321*, 554.
(11) Sales, B. C.; Mandrus, D. G.; Chakoumakos, B. C. In *Recent Trends in Thermoelectric Materials Research II, Semiconductors and Semimetals*; Tritt, T. M., Ed.; Academic Press: San Diego, 2000; Vol. 69, pp 1−36.
(12) Morelli, D. T.; Meisner, G. P. *J. Appl. Phys.* **1995**, *77*, 3777.
(13) Uher, C. In *Recent Trends in Thermoelectric Materials Research II, Semiconductors and Semimetals*; Tritt, T. M., Ed.; Academic Press: San Diego, 2000; Vol. 69, pp 139−253.
(14) Kuznetsov, V. L.; Kuznetsova, L. A.; Rowe, D. M. *J. Phys.: Condens. Matter* **2003**, *15*, 5035.
(15) Nolas, G. S.; Cohn, J. L.; Slack, G. A. *Phys. Rev. B* **1998**, *58*, 164.
(16) Nolas, G. S.; Kaeser, M.; Littleton, R. T.; Tritt, T. M. *Appl. Phys. Lett.* **2000**, *77*, 1855.
(17) Morelli, D. T.; Meisner, G. P.; Chen, B. X.; Hu, S. Q.; Uher, C. *Phys. Rev. B* **1997**, *56*, 7376.
(18) Lamberton, G. A.; Bhattacharya, S.; Littleton, R. T.; Kaeser, M. A.; Tedstrom, R. H.; Tritt, T. M.; Yang, J.; Nolas, G. S. *Appl. Phys. Lett.* **2002**, *80*, 598.
(19) Chen, L. D.; Kawahara, T.; Tang, X. F.; Goto, T.; Hirai, T.; Dyck, J. S.; Chen, W.; Uher, C. *J. Appl. Phys.* **2001**, *90*, 1864.
(20) Puyet, M.; Lenoir, B.; Dauscher, A.; Dehmas, M.; Stiewe, C.; Muller, E. *J. Appl. Phys.* **2004**, *95*, 4852.
(21) Zhao, X. Y.; Shi, X.; Chen, L. D.; Zhang, W. Q.; Zhang, W. B.; Pei, Y. Z. *J. Appl. Phys.* **2006**, *99*, 053711.
(22) Pei, Y. Z.; Chen, L. D.; Zhang, W.; Shi, X.; Bai, S. Q.; Zhao, X. Y.; Mei, Z. G.; Li, X. Y. *Appl. Phys. Lett.* **2006**, *89*, 221107.
(23) Pei, Y. Z.; Yang, J.; Chen, L. D.; Zhang, W.; Salvador, J. R.; Yang, J. H. *Appl. Phys. Lett.* **2009**, *95*, 042101.
(24) Sales, B. C.; Chakoumakos, B. C.; Mandrus, D. *Phys. Rev. B* **2000**, *61*, 2475.
(25) Nolas, G. S.; Takizawa, H.; Endo, T.; Sellinschegg, H.; Johnson, D. C. *Appl. Phys. Lett.* **2000**, *77*, 52.
(26) Nolas, G. S.; Yang, J.; Takizawa, H. *Appl. Phys. Lett.* **2004**, *84*, 5210.
(27) Fukuoka, H.; Yamanaka, S. *Chem. Mater.* **2010**, *22*, 47.
(28) Keppens, V.; Mandrus, D.; Sales, B. C.; Chakoumakos, B. C.; Dai, P.; Coldea, R.; Maple, M. B.; Gajewski, D. A.; Freeman, E. J.; Bennington, S. *Nature* **1998**, *395*, 876.
(29) Hermann, R. P.; Jin, R. J.; Schweika, W.; Grandjean, F.; Mandrus, D.; Sales, B. C.; Long, G. J. *Phys. Rev. Lett.* **2003**, *90*, 135505.
(30) Yang, J.; Zhang, W.; Bai, S. Q.; Mei, Z.; Chen, L. D. *Appl. Phys. Lett.* **2007**, *90*, 192111.
(31) Bai, S. Q.; Pei, Y. Z.; Chen, L. D.; Zhang, W. Q.; Zhao, X. Y.; Yang, J. *Acta Mater.* **2009**, *57*, 3135.
(32) Salvador, J. R.; Yang, J.; Wang, H.; Shi, X. *J. Appl. Phys.* **2010**, *107*, 043705.
(33) Zhao, W. Y.; Wei, P.; Zhang, Q. J.; Dong, C. L.; Liu, L. S.; Tang, X. F. *J. Am. Chem. Soc.* **2009**, *131*, 3713.
(34) Li, H.; Tang, X. F.; Zhang, Q. J.; Uher, C. *Appl. Phys. Lett.* **2009**, *94*, 102114.
(35) Dilley, N. R.; Bauer, E. D.; Maple, M. B.; Sales, B. C. *J. Appl. Phys.* **2000**, *88*, 1948.
(36) Shi, X.; Zhang, W.; Chen, L. D.; Yang, J.; Uher, C. *Acta Mater.* **2008**, *56*, 1733.
(37) Shannon, R. D. *Acta Crystallogr.* **1976**, *A32*, 751.
(38) Caillat, T.; Borshchevsky, A.; Fleurial, J.-P. *J. Appl. Phys.* **1996**, *80*, 4442.
(39) Shi, X.; Zhang, W.; Chen, L. D.; Yang, J. *Phys. Rev. Lett.* **2005**, *95*, 185503.
(40) Shi, X.; Zhang, W.; Chen, L. D.; Yang, J.; Uher, C. *Phys. Rev. B* **2007**, *75*, 235208.
(41) Yang, J.; Xi, L.; Zhang, W.; Chen, L. D.; Yang, J. H. *J. Elec. Mater.* **2009**, *38*, 1397.
(42) Shi, X.; Salvador, J. R.; Yang, J.; Wang, H. *J. Elec. Mater.* **2009**, *38*, 930.
(43) Morelli, D. T.; Caillat, T.; Fleurial, J. P.; Borshchevsky, A.; Vandersande, J.; Chen, B.; Uher, C. *Phys. Rev. B* **1995**, *51*, 9622.
(44) Yang, J.; Morelli, D. T.; Meisner, G. P.; Chen, W.; Dyck, J. S.; Uher, C. *Phys. Rev. B* **2003**, *67*, 165207.
(45) Shi, X.; Yang, J.; Wang, H.; Chi, M.; Salvador, J. R.; Yang, J.; Bai, S.; Zhang, W.; Chen, L.; Copley, J. R. D.; Leão, J. B.; Rush, J. J. *Phys. Rev. Lett.* (in review).
(46) Madsen, G. K. H.; Singh, D. J. *Comput. Phys. Commun.* **2006**, *175*, 67.
(47) Yang, J.; Li, H. M.; Wu, T.; Zhang, W. Q.; Chen, L. D.; Yang, J. H. *Adv. Funct. Mater.* **2008**, *18*, 2880.
(48) Chaput, L.; Pecheur, P.; Tobola, J.; Scherrer, H. *Phys. Rev. B* **2005**, *72*, 085126.
(49) Dyck, J. S.; Chen, W. D.; Uher, C.; Chen, L.; Tang, X. F.; Hirai, T. *J. Appl. Phys.* **2002**, *91*, 3698.
(50) Cahill, D. G.; Watson, S. K.; Pohl, R. O. *Phys. Rev. B* **1992**, *46*, 6131.
(51) Cahill, D. G.; Pohl, R. O. *Annu. Rev. Phys. Chem.* **1988**, *39*, 93.
(52) Dimitrov, I. K.; Manley, M. E.; Shapiro, S. M.; Yang, J.; Zhang, W.; Chen, L. D.; Jie, Q.; Ehlers, G.; Podlesnyak, A.; Camacho, J.; Li, Q. *Phys. Rev. B* **2010**, *82*, 174301.
(53) Zhang, L.; Grytsiv, A.; Rogl, P.; Bauer, E.; Zehetbauer, M. *J. Phys. D: Appl. Phys.* **2009**, *42*, 225405.
(54) Bai, S. Q.; Shi, X.; Chen, L. D. *Appl. Phys. Lett.* **2010**, *96*, 3.
(55) Slack, G. A. In *CRC Handbook of Thermoelectrics*; Rowe, D. M., Ed.; CRC: Boca Raton, FL, 1995; pp 407−440.
(56) Salvador, J. R.; Yang, J.; Shi, X.; Wang, H.; Wereszczak, A. A.; Kong, H.; Uher, C. *Philos. Mag.* **2009**, *89*, 1517.
(57) Wereszczak, A. A.; Ragan, M. E.; Pitt, P. J.; Wang, H.; Salvador, J. R.; Yang, J. *Ceram. Eng. Sci. Proc.* **2010**, *31*, 10.